International Scientific Conference 20 UNITECH 26

INTERNATIONAL SCIENTIFIC CONFERENCE
19-21 November 2026
GABROVO

CHARACTERIZATION OF THE 1-(4-methylbenzyl)-1*H*-imidazo[4,5-*f*][1,10]phenanthroline LIGAND VIA DENSITY FUNCTIONAL THEORY

G. Uluçam[1,*], S. E. Okan[2]

[1]*Chemistry Department, Faculty of Science, Trakya University, Edirne, Türkiye*
[2]*Physics Department, Faculty of Science, Trakya University, Edirne, Türkiye*
[*]*Corresponding author: e-mail: gulergul@trakya.edu.tr*

Abstract
Imidazophenanthroline-derived ligands, which have two heterocyclic rings, among these compounds, gather special attention in medicine and pharmacology; they demonstrate cytotoxic properties and selective inhibitory effects on diverse human cancer cell lines while exhibiting minimal toxicity to normal cells. The preliminary theoretical investigations of the ligands are beneficial for establishing ideal experimental parameters, and implementing safeguards against any experimental inaccuracies, that are crucial procedures. 1-(4-methylbenzyl)-1H-imidazo[4,5-f][1,10]phenanthroline, a new ligand generated from imidazophenanthroline, was modeled via density functional theory. The ligand was optimized with the B3LYP/6-311G++ (2d, p) basis set in the Gaussian G09w software suite. Then, the ligand's NMR and FT-IR spectra were computed based on the optimization. Alongside bond lengths, bond angles, and dihedral angles, the molecular electrostatic potential map, Mulliken atomic charges, dipole moments, and the energies of the highest occupied molecular orbital (HOMO) and lowest unoccupied molecular orbital (LUMO) were assessed. The imidazophenanthroline-derived ligand is expected to establish coordination interactions with metal salts; hence, it is regarded as a potential metal ion transporter or scavenger.

Keywords: *Imidazophenanthroline, HOMO-LUMO, MEP, DFT/B3LYP*

INTRODUCTION

Heterocyclic compounds with at least one donor atom such as nitrogen, oxygen, or sulfur, hold considerable importance in contemporary pharmaceutical research. The grouping of molecules holds major importance in pharmaceutical chemistry because of its tendency to interact with biological targets. These compounds demonstrate activity in a wide pharmacological spectrum, comprising antibacterial, antifungal, anticancer, anti-inflammatory, and antiviral drugs. Heterocyclic compounds exhibit a wide range of biological functions due to their ability to engage with specific binding sites on molecular targets [1-7]. In this respect, the imidazophenanthroline moiety, arising from the merger of the imidazole ring and phenanthroline, is a structure that captivates attention owing to its aromatic characteristics and polypharmacological potential. Imidazophenanthroline derivatives have been extensively reported in scientific papers showing an array of biological activities, notably antifungal, anticancer, antibacterial, and antiviral properties [8-10]. The therapeutic effects of these arrangements can typically be modified by different functional groups attached to the core structure. This gives the Imidazophenanthroline structure an appealing structural basis for the development of novel medicinal substances [11-13]. Currently, computational chemistry methodologies have emerged as powerful tools for assessing the structural and electrochemical characteristics of biologically active substances. Density Functional Theory (DFT) is particularly

This is an open access article licensed under Creative Commons Attribution 4.0 International
Print ISSN: 1313-230X, Online ISSN: 3033-1404

favored in theoretical chemistry due to its ability to accurately and economically predict the optimal structures and electrochemical characteristics of molecules [14-17].

In this context, the geometric structure of the ligand called 1-(4-methylbenzyl)-1*H*-imidazo[4,5-*f*][1,10] phenanthroline has been theoretically elucidated, and their optical, geometric, and chemical properties have been calculated. The ligand was optimized with the B3LYP/6-311G++ (2d, p) basis set in the Gaussian G09w software suite [17]. Then, the ligand's NMR and FT-IR spectra were computed based on the optimization. Alongside bond lengths, bond angles, and dihedral angles, the molecular electrostatic potential map, Mulliken atomic charges, dipole moments, and the energies of the highest occupied molecular orbital (HOMO) and lowest unoccupied molecular orbital (LUMO) were assessed.

FINDINGS

Molecular Geometry

The ligand was optimized in the gas phase, and its minimization energy, dipole moment, and polarizability were calculated as -1029.184705 au, 7.196626 Debye, and 290.880108 au, respectively. The ligand has the C1 symmetry group, and the structure of the ligand is shown in Fig. 1.

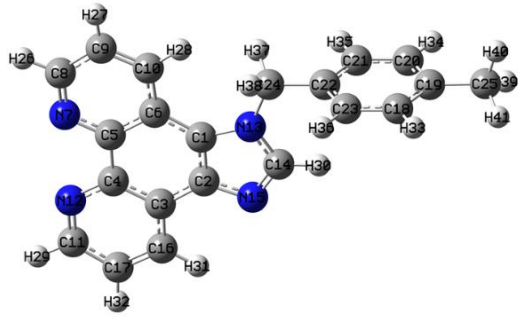


Fig. 1. *The suitable structure of the ligand with the lowest theoretically calculated energy.*

The distances between the atoms of the ligand are presented in Table 1, while the significant bond and dihedral angles are detailed in Table 2.

Table 1. *Interatomic bond lengths of the ligand*

Selected Bond Lengths (Å)	Selected Bond Lengths (Å)
1.0869 (C11-H29)	1.0922 (C24-H38)
1.3195 (N12-C11)	1.5085 (C24-C22)
1.3474 (C4- N12)	1.3945 (C22-C23)
1.4158 (C3-C4)	1.0848 (C24-H36)
1.4299 (C2-C3)	1.3896 (C23-C18)
1.3882 (C1-C2)	1.0845 (C18-H33)
1.3912 (N13-C1)	1.3964 (C18-C19)
1.3707 (N13-C14)	1.5072 (C19-C25)
1.0772 (C14-H30)	1.0913 (C25-H39)
1.4717 (N13-C24)	1.0945 (C25-H40)
1.0922 (C24-H37)	1.0913 (C25-H41)

In the ligand, the bond length of C24-N13 measures 1.47 Å (indicative of a single bond), the bond length of C24-C22 is 1.51 Å (characteristic of a carbon-carbon single bond), and the carbon-hydrogen bonds in the CH_3 and CH_2 groups are approximately 1.092 Å. The carbon-hydrogen bonds in phenanthroline and benzene were measured to be approximately 1.083 Å, but those in the imidazole ring were measured to be around 1.077 Å. Dihedral angles interfere with the planar configuration of the ligand's tail.

Table 2*. Bond and dihedral angles between atoms of the ligand*

Selected Bond Angles (º)	Selected Dihedral Angles (º)
107.39 (H41-C25-H40)	-151.12 (H41-C25-C19-C20)
110.90 (H40-C25-C19)	89.33 (H40-C25-C19-C20)
121.03 (C25-C19-C20)	-178.57 (C25-C19-C20-C21)
119.51 (C19-C20-H34)	-0.25 (C19-C20-C21-C22)
121.10 (C19-C20-C21)	179.82 (H34-C20-C21-C22)
119.39 (H34-C20-C21)	0.083 (H34-C20-C21-H35)
120.80 (C21-C22-C24)	-30.85 (C21-C22-C24-H37)
109.46 (C22-C24-H37)	-148.78 (C21-C22-C24-H38)
113.78 (C22-C24-N13)	-0.002 (C22-C24-N13-C14)
126.32 (C24-N13-C14)	0.0009 (C24-N13-C14-H30)
121.44 (N13-C14-H30)	179.99 (H30-C14-N15-C2)
113.37 (N13-C14-N15)	-179.99 (C14-N15-C2-C3)
111.07 (N15-C2-C1)	
127.23 (N15-C2-C3)	

Mulliken Atomic Charge Distribution

The arrangement of electrons within a molecule is influenced by the distribution of Mulliken atomic charges. The Mulliken distribution for the examined molecule is illustrated in Fig. 2. The color scheme indicates that red signifies the most substantial negative charge (-0.626), whilst

green denotes the most significant positive charge (0.626).

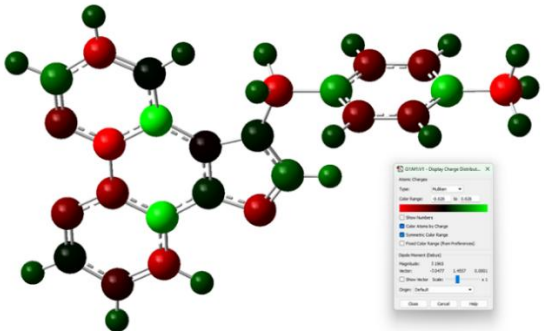


Fig. 2. *Mulliken atomic charges of the ligand*

In this configuration, the nitrogen atom (N13) attached to the tail has a positive charge of 0.066892, while the other nitrogen atoms (N7, N12, N15) have negative charges of -0.242776, -0.275715, and -0.371887, respectively

HOMO-LUMO Analysis and Electronic Properties

Frontier molecular orbitals (FMO) are dominant in determination the electrical and optical characteristics of a molecule. The energy difference between HOMO and LUMO provides information on the molecular properties. The diminished energy disparity leads to a more polarized molecule. When the energy disparity is significant, the molecule is characterized as hard, indicating diminished reactivity. The energy of HOMO pertains to Ionization Potential (IP), whereas the energy of LUMO relates to Electron Affinity (EA).

Table 3*. Electronic structure parameters of the ligand and their values*

Parameter	*Value*
E_{HOMO} (eV)	-5.97535
E_{LUMO} (eV)	-1.59404
ΔE (eV)	4.38131
IP (eV)	5.97535
EA (eV)	1.59404
χ(eV)	3.78470
μ (eV)	-3.78470
η (eV)	2.19066
σ (eV^{-1})	0.45648
ω	3.26932

IP:-EHOMO, EA:-ELUMO, ΔE=ELUMO-EHOMO,

$\chi = (IP+EA)/2$, $\mu = -\chi$, $\eta = (IP-EA)/2$, $\sigma = 1/\eta$, $\omega = \mu^2/2\eta$

Furthermore, electronegativity (χ), chemical potential (μ), chemical hardness (η), electrophilicity index (ω) and chemical softness (σ) were derived from FMO energies [18, 19]. The HOMO-LUMO energy of the ligand is shown in Fig. 3. The molecular electrical characteristics derived from HOMO and LUMO energies are presented in Table 3. The Gaussian output values, expressed in atomic units (a. u.), were subsequently transformed into electrostatic units (1 a. u. = 27.211396 eV).

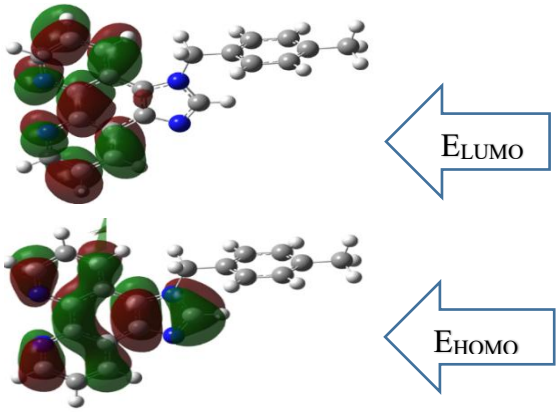


Fig. 3. *HOMO and LUMO three-dimensional representations and energy values*

The HOMO energy, indicative of the molecule's ability to donate electrons, is -5.97535 eV, while the LUMO energy, indicating its electron removal potential, is -1.59404 eV; thus, the energy gap is calculated to be 4.38131 eV. The relatively small energy gap promotes the chemical synthesis of the molecule [20].

Molecular Electrostatic Potential Surface

By comparing the results presented in Table 3 with those derived from a similar molecule in an earlier investigation, their electrical characteristics are quantitatively similar [19, 21]. The value of ω=3.26932 eV, denoting biological activity, is comparable, which has an electrophilic index of ω=2.931 eV. The chemical softness metric σ, which quantifies chemical reactivity, is similarly applicable [21].

Regions with a lower electron density are demonstrated in yellow, while neutral areas

are represented in green. In the MEP map of the ligand depicted in Fig. 5, the color gradients of the electronic potential surfaces range from -7.796 e-2 (red) to 7.796 e-2 (blue). Accordingly, the geometric location and energy of bonding in interactions with metals are determined by the red regions.

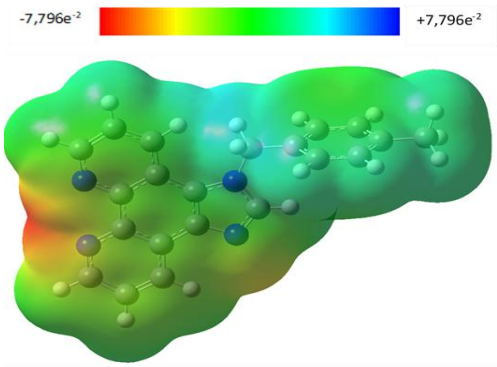


Fig. 4. *Molecular electrostatic potential map of the ligand.*

Theoretical NMR spectrums

The GIAO technique was used to calculate the theoretical ^{1}H- and ^{13}C-NMR chemical shifts, the spectra of which are presented in Fig. 5. and Fig. 6. Chemical shift values for the protons in the ligand were determined as follows: phenanthroline protons between 9.50 and 7.66 ppm, the imidazole proton (H30) at 7.11 ppm, the CH_2 proton (H37, H38) at 5.64, 5.64 ppm, and the CH_3 protons (H39, H40, H41) at 2.39, 2.70 and 2.39 ppm.

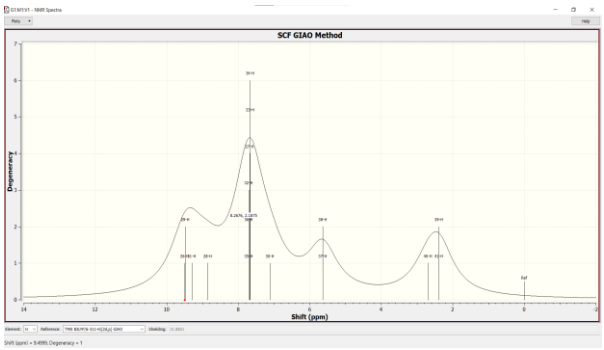


Fig. 5. *Theoretical ^{1}H-NMR spectra*

For the carbons in the ligand, chemical shift values were determined as follows: aromatic carbons between 153.1 and 124.0 ppm, the imidazole carbon (C14) at 143.7 ppm, the CH2 carbon (C24) at 56.8 ppm, and the CH3 carbon (C25) at 22.1 ppm [22].

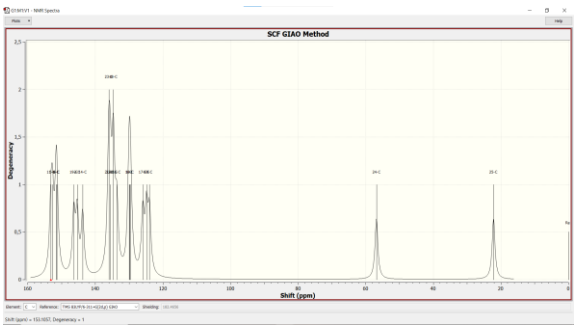


Fig. 6. *Theoretical ^{13}C-NMR spectra*

Theoretical FTIR spectrums

The computed vibration spectrum is illustrated in Fig. 7. It is widely recognized that minor discrepancies may exist between the vibration frequencies predicted by quantum chemical techniques, such as DFT, and those observed experimentally. The discrepancies are reduced by multiplying the theoretically derived frequencies by 0.9613, the appropriate scaling factor for the 6-311G++ (2d, p) basis set [22]. Detailed potential energy distribution (PED) analysis was performed using the VEDA program [23].

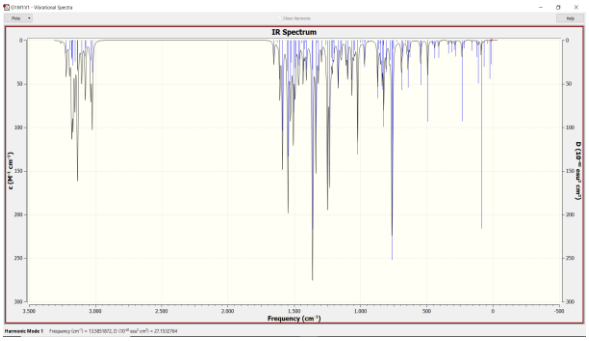


Fig. 7. *Theoretical FTIR spectrum*

An examination of the ligand's theoretical FTIR spectrum revealed a total of 117 vibrational modes, comprising 40 stretching modes (ν), 39 bending modes (δ), and 38 torsional modes (γ). All vibration values are unscaled values.

All ν(CH) stretching modes appear in the 3261–3024 cm^{-1} range (specifically, imidazole ν(C14H30) at 3261 cm^{-1}; CH_3

asymmetric ν(C25H39, C25H40, C25H41) at 3077 cm^{-1}; CH_3 symmetric ν(C25H39, C25H40, C25H41) at 3024 cm^{-1}; CH_2 asymmetric ν(C24H37, C224H38) at 3073 cm^{-1}; and CH_2 symmetric ν(C24H37, C224H38) at 3035 cm^{-1}). Selected vibrational modes that are stretching, in-plane bending, and out-of-plane bending vibrations are presented. The ν (N15C14) stretching mode is located at 1507 cm^{-1}, the ν (N7C8) and ν (N12C11) stretching modes at 1294 cm^{-1}, and the ν (C2C3) stretching mode at 1546 cm^{-1}. Meanwhile, the δ bending mode (for H34C20C21, H33C18C23, H36C23C22, and H35C21C22) is at 1654 cm^{-1}. The δ bending mode for N13C14N15 is at 1208 cm^{-1}, and the same mode for H26C14N15 is at 1468 cm^{-1}. Additionally, the vibrations of H29C11N12C4, H31C16C3C4, and H32C17C16C3 are γ torsional appears at the same frequency of 1000 cm^{-1}. The γ torsion of C2N15C14N13) is at 642 cm^{-1}, and that of C25C18C20C19 and C23C21C24C22 is at 338 cm^{-1}. A comparison of all calculated vibrational values with those from the literature indicates consistency [14, 22].

CONCLUSION

By minimizing the energy of the called 1-(4-methylbenzyl)-1*H*-imidazo[4,5-*f*][1,10] phenanthroline in the gas phase, the geometric characteristics including interatomic bond lengths, bond angles, and dihedral angles were determined. The NMR and FT-IR spectra were computed utilizing the optimized geometry, yielding results consistent with the relevant literature. The ligand's electronegativity, chemical potential, chemical softness, chemical hardness, and electrophilicity index were determined using HOMO-LUMO energies. The MEP map indicated that the areas containing the ligand's nitrogen will display nucleophilic characteristics. The insights acquired here regarding the ligand will facilitate its synthesis.

REFERENCES

[1] Dunya YF, Khalid J.Al-A. Synthesis and spectral characterization of some metal complexes with new heterocyclic azo imidazole dye ligand and study biological activity as anticancer. Journal of Molecular Structure 2023;1271-1340891.

[2] Dongli L, Panpan W, Ning S, Yu-Jing L, Wing-Leung W, Zhiyuang F, Kun Z. The Diversity of Heterocyclic N- oxide Molecules: Highlights on their Potential in Organic Synthesis. Catalysis and Drug Applications Results in Chemistry 2019;23:5:616-627.

[3] Chopra PN, Sahu JK. Biological Significance of Imidazole-based Analogues in New Drug Development. Curr. Drug Discov. Technol 2020;17:574–584.

[4] Rossi R, Ciofalo M. An Updated Review on the Synthesis and Antibacterial Activity of Molecular Hybrids and Conjugates Bearing Imidazole Moiety. Molecules 2020; 25:5133.

[5] Daraji DG, Prajapati NP, Patel HD. Synthesis and Applications of 2- Substituted Imidazole and Its Derivatives: A Review. J. Heterocyclic Chem 2019;56.2299–2317.

[6] Zhang L, Peng XM, Damu GLV, Geng RX, Zhou CH. Comprehensive Review in Current Developments of Imidazole-Based Medicinal Chemistry. Med. Res. Rev 2014;34:340–437.

[7] Verma A, Joshi S, Singh D. Imidazole: Having Versatile Biological Activities. Journal of Chemistry 2013;329412:12 pages,;Article ID 329412.

[8] Gratal P, Arias-P´erez MS, Gude L. 1H-imidazo [4,5-f] [1,10] phenanthroline carbohydrate conjugates: synthesis, DNA interactions and cytotoxic activity, Bioorganic Chemistry 2022; 125:105851.

[9] Sun DD, Wang WZ, Mao JW, Mei WJ, Liu J. Imidazo[4,5-f][1,10] phenanthroline derivatives as inhibitor of c-myc gene expression in A549 cells via NF-B pathway. Bioorg. Med. Chem. Lett 2012;22:102–105.

[10] Bergamo A, Dyson PJ, Sava G. The mechanism of tumour cell death by metal-based anticancer drugs is not only a matter of DNA interactions. Coordin, Chem. Rev 2018;360:17–33.

[11] Kar B, Das U, De SD, Pete S, Sharma AS, Nilmadhab R, Ashok Kumar SK, Panda D,

Paira P. GSH-resistant and highly cytoselective ruthenium(ii)-p-cymene-(imidazo[4,5-f][1,10] phenanthrolin-2-yl)phenol complexes as potential anticancer agents. Dalton Trans 2021;50:10369–10373.

[12] De S, Kumar RS, Gauthaman A, Ashok Kumar SK, Paira P, Moorthy A, Banerjee S. Luminescent ruthenium(II)-para-cymene complexes of aryl substituted imidazo-1,10-phenanthroline as anticancer agents and the effect of remote substituents on cytotoxic activities. Inorgan. Chim. Acta 2021;515: 120066.

[13] Lin J, Zhou S, Xian H, Chen W, Zhang Y, Zhang W, Guan Z, Mei W. Imidazolebased phenanthroline derivatives induce DNA damage-mediated apoptosis to suppress hepatocellular carcinoma. J. Holis. Integ. Pharm 2022);3:(2) 177–189.

[14] Al-Otaibi JS, Al-Wabli RI. Vibrational spectroscopic investigation (FT- IR and FT-Raman) using ab initio (HF) and DFT(B3LYP) calculations of 3-ethoxymethyl-1,4-dihydroquinolin-4-one. Spectrochim Acta A Mol Biomol Spectrosc 2015;137:7-15.

[15] Ulucam G, Turkyilmaz M. Synthesis, Structural Analysis, and Biological Activities of Some Imidazolium Salts. Bioinorganic Chemistry and Applications 2018;1:1-12

[16] Uluçam G, Okan SE, Aktaş Ş, Öğretmen GP. Characterization of dinaphthosulfoxide molecule. Journal of Molecular Structure 2015; 1102:146-152.

[17] Foresman JB, Frisch AE. Exploring chemistry with electronic structure methods (2 ed.). Wallingford, CT: Gaussian, Inc., 1996.

[18] Altürk S, Avcı D, Tamer Ö, Atalay Y. 1H–pyrazole–3–carboxylic acid: Experimental and computational study. Journal of Molecular Structure 2018;1164: 28-36.

[19] Manikandan M, Rajesh P, Ramasamy P. Crystal growth, structural, optical, vibrational analysis, Hirshfeld surface and quantum chemical calculations of 1, 3, 5-triphenylbenzene single crystal. Journal of Molecular Structure 2019;1195:659-669.

[20] Singaravelan K, Chandramohan A, Madhankumar S, Enoch M, Vinitha G. Structural characterization, computational and biological studies of a new third order NLO (1:1) organic adduct: 2-Aminopyrimidine: 3-nitrophthalic acid. Journal of Molecular Structure 2019;1194:57-65.

[21] Uluçam G. Theoretical Characterization Of A Imidazophenanthroline Derived Ligand By The Density Functional Method, International Scientific Conference, 17-18 November 2023, Gabrovo.

[22] Uluçam G, Bagcı U, Şuekinci Yılmaz A, Yentürk B. Schiff-base ligands containing phenanthroline terminals: Synthesis, characterization, biological activities and molecular docking study. Spectrochimica Acta Part A: Molecular and Biomolecular Spectroscopy 2022;279:121429.

[23] Turkyilmaz M, Uluçam G, Aktaş Ş, Okan SE. Synthesis and characterization of new N-heterocyclic carbene ligands: 1, 3-Bis (acetamide) imidazol-3-ium bromide and 3-(acetamide)-1-(3-aminopropyl)-1H-imidazol-3-ium bromide. Journal of Molecular Structure 2017;1136:263-270.